

STUDIES OF STABILITY AND CONTROL OF
WINGED REENTRY CONFIGURATIONS

By Robert W. Rainey and William H. Close
Langley Research Center

SUMMARY

L
1
0
4
0

A study of the static stability and control problem areas of winged reentry vehicles capable of maximum lift-drag ratios of about 2 at hypersonic speeds has been made. Throughout the Mach number and angle-of-attack ranges of the tests, it appears that the center-of-gravity location will be a compromise between operation at maximum lift-drag ratio at subsonic speeds and at maximum lift at hypersonic speeds, where the aerodynamic center is significantly aft of its location at subsonic speeds. At maximum lift at hypersonic speeds, combinations of nose and flap deflections will trim the vehicle with reasonable longitudinal stability, and the static directional stability may be increased by use of wing-tip-fin roll-out. At hypersonic speeds, care must be exercised to tailor the forward portions of the vehicle in order to avoid longitudinal and directional instability in the low-angle-of-attack range; at low angles of attack the longitudinal control effectiveness is very low and auxiliary control devices may be required.

INTRODUCTION

A study has been made of several static longitudinal, directional, and lateral stability and control problems associated with winged reentry vehicles capable of maximum lift-drag ratios of about 2 at hypersonic speeds. This study was carried out at speeds from subsonic to a Mach number of 18 and in the angle-of-attack range from 0° to that for maximum lift (near 55°). Several problem areas are discussed herein along with possible solutions.

Preceding page blank

SYMBOLS

C_L	lift coefficient, $\frac{\text{Lift}}{q_\infty S_{\text{WING}}}$	
C_l	rolling-moment coefficient, $\frac{\text{Rolling moment}}{q_\infty S_{\text{WING}} b}$	
C_m	pitching-moment coefficient, $\frac{\text{Pitching moment}}{q_\infty S_{\text{WING}} \bar{c}}$	L 1 0 4 0
C_N	normal-force coefficient, $\frac{\text{Normal force}}{q_\infty S_{\text{WING}}}$	
C_n	yawing-moment coefficient, $\frac{\text{Yawing moment}}{q_\infty S_{\text{WING}} b}$	
$C_{l\beta}$	effective dihedral parameter, $\frac{\partial C_l}{\partial \beta}$, per deg	
$C_{n\beta}$	static directional stability parameter, $\frac{\partial C_n}{\partial \beta}$, per deg	
$(\Delta C_{n\beta})_{\text{fin}}$	fin contribution to static directional stability parameter, per deg	
$\frac{\partial C_m}{\partial C_N}$	static longitudinal stability parameter	
b	wing span, in.	
\bar{c}	mean aerodynamic chord, in.	
L/D	lift-drag ratio	
M	Mach number	
$\frac{(p_r/p_\infty) - 1}{(p_i/p_\infty) - 1}$	real-gas pressure parameter, ratio of real-gas to ideal-gas pressure coefficients	

p	static pressure
q	dynamic pressure, lb/sq in.
S_{FLAP}	flap planform area, sq in.
S_{FIN}	single fin area, sq in.
S_{NOSE}	nose planform area, sq in.
S_{WING}	total wing planform area, sq in.
α	angle of attack, deg
β	angle of sideslip, deg
δ_n	nose-panel-deflection angle, deg
δ_f	flap-panel-deflection angle, deg
ϕ	fin roll-out angle referenced from the vertical plane

Subscripts:

MAX	maximum
t	trim
∞	free-stream conditions
r	real-gas conditions
i	ideal-gas conditions

DISCUSSION

Longitudinal Stability and Control

Angles of attack for maximum L/D or less.- The stability of several wings and winged vehicles is presented in figure 1 for an angle of attack of 10° which is approximately that for maximum L/D. The aerodynamic-center location relative to the mean aerodynamic chord is plotted against Mach number. These results are from references 1 to 5 and unpublished results from Boeing Airplane Co. In the lower portion

of the figure are presented results from tests of simple, symmetrical delta wings; these results show that there is a large rearward shift in aerodynamic center in the transonic speed range. At Mach numbers above about 1, the aerodynamic center is located close to 50-percent mean aerodynamic chord which is the centroid of area. However, for the four reentry vehicles shown, which have bodies and fins in combination with wings of unsymmetrical airfoil section, large aerodynamic-center shifts are exhibited throughout the transonic and supersonic speed ranges. At hypersonic speeds the aerodynamic-center location is ahead of the 50-percent mean aerodynamic chord and is invariant with Mach number. Additional tests have been made for two of the configurations reported in reference 1 in the air nozzle ($M_\infty = 9.6$) and the helium nozzles ($M_\infty \approx 10$ and 18) of the Langley 11-inch hypersonic tunnel by Charles L. Ladson; whereas at a Mach number near 18, results are also available from AEDC Hotshot 1 using air (ref. 2). It can be seen that there is little effect of the variation in fluid properties upon the stability of the vehicles tested. Furthermore, for these vehicles, the results for $M = 6.8$ and 9.6 are representative of the results for higher Mach numbers. It is obvious that from a stability consideration for these vehicles, the results for the delta wings should not be depended upon. In general, the variation in the aerodynamic-center location with Mach number is similar for the four reentry vehicles. In addition, the trend in center-of-pressure location is quite similar to the aerodynamic-center shifts shown in this figure, and the problem of providing sufficient control to trim the vehicle even at low lift coefficients through the supersonic-speed range is evident. At angles of attack higher than that of 10° shown in figure 1 and at hypersonic speeds, the aerodynamic center and center of pressure move rearward, and, generally speaking, the center-of-gravity location would involve a compromise between the high-angle-of-attack trim at hypersonic speeds and the low-angle-of-attack stability at subsonic speeds. From considerations for subsonic speeds, a center-of-gravity location at 42-percent mean aerodynamic chord appears reasonable and will be used for the remainder of this presentation.

At angles of attack lower than that of 10° shown in figure 1, the shape of the forward portions of the vehicle and the wing airfoil section have a marked influence on the stability. Examples of this are presented in figure 2, in which for a Mach number of 9.6, the pitching moment is plotted against normal force for two of the vehicles of figure 1 for flap deflections of 0° and -10° for the upper vehicle and for 0° for the lower. In the higher angle-of-attack range, the upper vehicle in stable and flap effectiveness is high. However, as the angle of attack is reduced below that for $(L/D)_{MAX}$ the large variations in the downloads on the fuselage nose and airfoil section with α resulted in marked instability. Furthermore, the flap effectiveness is very low. Modification of the fuselage nose from the triangular cross section of the upper vehicle to a higher fineness-ratio, "D" cross section of the

L
1
0
4
0

lower vehicle along with a reduction in the airfoil thickness was sufficient to alleviate the longitudinal instability; however, although the results are not presented herein, the problem of low flap effectiveness is still prevalent. Other results not reported herein show that for flap deflections up to -45° , the flap effectiveness is still quite low for flaps with an area approximately 10 percent of the wing area. Consequently, larger flaps or auxiliary devices or both appear to be in order. It should be noted for figure 2, as was pointed out for figure 1, that the body, and to some degree the fins, influence strongly the longitudinal characteristics in the low angle-of-attack range and wing-alone data are not indicative of the complete-vehicle characteristics.

Angles of attack near maximum lift.- At the angles of attack greater than about 25° , the effects of components on top of the wing are essentially nonexistent, and insofar as the vehicle characteristics are concerned, the complete vehicle may be simulated by a simple wing alone. In order to examine the high angle-of-attack trim problem at hypersonic speeds, an investigation was undertaken with a 70° swept, flat-plate delta wing at $M_\infty = 6.7$; the pitching-moment coefficients of this wing about the 42-percent mean aerodynamic chord are plotted in figure 3 against angle of attack for flap deflections of 0° , -10° , and -20° . The test-point symbols denote the measured results, and the lines denote the results from computations which utilized the correlation of measured delta-wing data at angles of attack in excess of leading-edge-shock detachment. (See ref. 6.) For the wing with the undeflected flap, the large negative pitching moments in the maximum-lift range which must be trimmed out are evident; consequently, a relatively large flap is in order. For the results presented herein the flap area was 19 percent of the wing area. The use of flap deflection at these angles of attack provides sizable increments in pitching moments, and as expected, the effects of flap deflection are destabilizing. The computations underestimate somewhat both the pitching-moment increments and the destabilizing effects of negative flap deflection in the range of $C_{L,MAX}$. Larger negative flap deflections will provide trim in the maximum-lift range but with a further decrease in the stability. The longitudinal stability may be increased somewhat by the use of nose deflection as shown in figure 4, in which the results show the increase in stability throughout the angle-of-attack range along with the increments in pitching moment which are smaller at the higher angles of attack. The computations overestimated the moment increments and underestimated the stability increase near maximum lift.

From a stability and control standpoint, it appears feasible to consider the combined use of nose and flap deflection to provide trim with stability at angles of attack near maximum lift. In figure 5 are summarized some of the high-angle-of-attack trim characteristics of the 70° swept wing at $M_\infty = 6.7$. The computed results, shown as solid lines,

are presented as the trim stability parameter $(\partial C_m / \partial C_N)_t$ plotted against the trim angle of attack α_t for nose deflections of 0° , 5° , and 10° . Along each line of constant nose deflection, the flap deflection angle varies from a small negative value to -40° . The dashed lines are the computed contours of constant trim lift coefficient. For these trim conditions, an increase in nose deflection angle increased the vehicle stability as was noted previously for the untrimmed case (fig. 4). By use of combined nose and flap deflections, it is possible to provide trim with stability at maximum lift (fig. 5). The maximum value of trim C_L is 0.62 based on total planform area including flaps. If the center of gravity could be located more rearward, trim C_L could obviously be increased. However, such a rearward shift in center of gravity would not necessarily reduce the overall stability inasmuch as less destabilizing negative flap deflections would be needed to trim. Experimental trim results, shown in figure 5 by the test-point symbols, have been obtained for several combinations of nose and flap deflections (ref. 6). Arrows from each test-point symbol connect the experimental point with its comparative computed point. In general, good agreement exists between the experimental and computed results except that the computations yield slightly higher stability. The highest measured trim lift coefficient obtained throughout this experimental investigation was 0.63 while the highest value of lift coefficient measured for the undeflected, untrimmed delta wing was 0.72. Of major interest also are the trim characteristics at higher Mach numbers, and in figure 6 are summarized the results of computations for a Mach number of 18 for the same 70° swept delta wing utilizing the computational method of reference 6 for ideal-gas conditions. These computed results are similar to those at $M_\infty = 6.7$ (fig. 5) except that the value of maximum trim lift is slightly lower. Included for comparison is the computed value of maximum trim lift for a vehicle with a wing loading of 25 lb/sq ft at an altitude of 242,000 feet where the real-gas effects have been approximated as follows:

The method of reference 6 for computing longitudinal stability for ideal-gas conditions was extended to the approximate real-gas conditions by the use of references 7 and 8. For the two-dimensional case of reference 7 up to shock detachment and for the normal-shock case of reference 8, a variation with flow deflection angle was obtained for the parameter $\frac{(p_r/p_\infty) - 1}{(p_i/p_\infty) - 1}$ for the case of a Mach number of 18 and an altitude of 242,000 feet (1956 ARDC model atmosphere). At the various panel flow-deflection angles, the individual ideal-gas panel pressure coefficients previously obtained were multiplied by this real-gas pressure parameter and the product is the approximate real-gas pressure coefficient.

These approximate real-gas effects did not alter the value of the maximum trim lift appreciably as compared with the ideal-gas value although the angle of attack at which it occurred was significantly higher and the control geometry required was slightly altered.

It should be emphasized that while effects of variation in nose deflection have been discussed herein, a reentry vehicle would utilize a fixed nose. Care must be exercised in the selection of such a nose with regard to exceeding the temperature limitation on this deflected area and with regard to the reduction in stability produced by the nose at angles of attack near $(L/D)_{MAX}$ or lower. Past experience (ref. 9) indicates that about 5° of nose deflection in combination with a small negative flap deflection will trim a similar vehicle at angles of attack in the range of $(L/D)_{MAX}$ with essentially no performance penalty and with reasonable longitudinal stability. The results presented herein (figs. 5 and 6) indicate that these angles of nose deflection may be used in combination with large negative flap deflections to provide trim with stability at maximum lift.

Directional and Lateral Stability

Basic stability derivatives.- With regard to directional and lateral stability, results from tests of two vehicles (from ref. 1 and unpublished results from Boeing Airplane Co.) are presented in figure 7 for an angle of attack approximately that for $(L/D)_{MAX}$. The static $C_{n\beta}$ and $C_{l\beta}$ (body axes) are presented as functions of Mach number. For both vehicles the decay in $C_{n\beta}$ with Mach number increase due to the reduction in tip-fin effectiveness is evident. For this type of vehicle, the positive value of $C_{l\beta}$ can be removed by a small amount of dihedral of the lower wing surface. Angle of attack also has an appreciable influence on directional and lateral stability as seen in figure 8. At low angles of attack the static $C_{n\beta}$ increased with α as a result of the reduction in the destabilizing influence of the fuselage nose. At higher angles of attack, the effectiveness of the tip fins falls off and static directional instability results. However, for these vehicles with highly swept wings, $C_{l\beta}$ becomes large negatively and may offset the directional instability for the dynamic case.

Method to improve static $C_{n\beta}$.- If it is desirable to have positive values of static $C_{n\beta}$ at these high angles of attack, one method of improving static $C_{n\beta}$ is the use of fin roll-out (fig. 9). The fin

roll-out angle ϕ is that angle between the plane of the fin and the vertical. The use of roll-out causes the maximum deflection angle of the flow relative to the fin to occur at higher angles of attack; thus, the initiation of $C_{n\beta}$ decay is delayed to a higher angle of attack. It is seen that in this angle-of-attack range, fin roll-out may be used to nullify the familiar $C_{n\beta}$ decay shown for $\phi = 0^\circ$ and to produce an invariant or an increasing $C_{n\beta}$ contribution of the fins with α increase. Of course, with fin roll-out there is an input to the pitching moment of the vehicle, and an increment in negative flap deflection $\Delta\delta_f$ is necessary to overcome this pitching-moment input and to retrim the vehicle as shown by the dashed curves. In this regard the longitudinal trim limit at which the flaps become streamwise and lose their effectiveness is shown by the cross-hatched boundary in this figure. From consideration of cross-control effects due to rudder deflection, roll-out should be limited to small amounts, probably about 10° or 15° . Also roll-out of this magnitude would require only about 2° additional negative flap deflection to retrim the vehicle at hypersonic speeds and would improve the longitudinal stability at subsonic speeds by about 2-percent mean aerodynamic chord.

L
1
0
4
0

CONCLUDING REMARKS

In conclusion, several aspects and problems of major importance to the stability and control of winged reentry vehicles have been discussed along with possible solutions for the problem areas. Although the magnitudes of the problems for specific vehicles would undoubtedly be altered from those contained within this generalized discussion, the principles behind which these solutions were reached should be applicable.

REFERENCES

1. Ladson, Charles L., Johnston, Patrick J., and Trescott, Charles D., Jr.: Effects of Planform Geometry on the Aerodynamic Characteristics of a Hypersonic Glider at Mach Numbers Up to 9.6. NASA TM X-286.
2. Wallace, A. R., and Swain, W. N.: Force, Heat Transfer, and Pressure Distribution Tests of Martin-Bell Dyna-Soar Glider Models at Mach Numbers 15 - 21. AEEDC TN 60-25 (Contract No. AF 40(600)-800), Arnold Eng. Dev. Center, Feb. 1960.
3. McDevitt, John B., and Rakich, John V.: The Aerodynamic Characteristics of Several Thick Delta Wings at Mach Numbers to 6 and Angles of Attack to 50°. NASA TM X-162, 1960.
4. Mueller, James N.: An Investigation of the Effect of Varying the Maximum-Thickness Position Upon the Aerodynamic Characteristics of a Series of $3\frac{1}{2}$ -Percent-Thick Delta Wings. NACA RM L55D26, 1955.
5. Shanks, Robert E.: Effects of Wing Crank and Sweepback on the Low Subsonic Stability and Control Characteristics of a Model of a Hypersonic Boost-Glide Type Airplane. NASA TM X-181, 1960.
6. Close, William H.: Hypersonic Longitudinal Trim, Stability, and Control Characteristics of a Delta-Wing Configuration at High Angles of Attack. NASA TM X-240, 1960.
7. Trimpi, Robert L., and Jones, Robert A.: A Method of Solution With Tabulated Results for the Attached Oblique Shock-Wave System for Surfaces at Various Angles of Attack, Sweep, and Dihedral in an Equilibrium Real Gas Including the Atmosphere. NASA TR R-63, 1960.
8. Huber, Paul W.: Tables and Graphs of Normal-Shock Parameters at Hypersonic Mach Numbers and Selected Altitudes. NACA TN 4352, 1958.
9. Rainey, Robert W., Fetterman, David E., Jr., and Smith, Robert: Summary of Static Stability and Control Results of a Hypersonic Glider Investigation. NASA TM X-277, 1960.

L
1
0
4
0

TABLE I.- AXISYMMETRIC STAGNATION-POINT HEAT-TRANSFER PARAMETER

370

$$[N_{Le} = 1]$$

Solution	Reference	Gas	Transport properties		A	m
			μ	N_{Pr}		
Sibulkin	30	Incompressible	Constant	Constant	0.763	0.5
Beckwith	31	Perfect compressible	Sutherland	Constant	.76	.4
Fay and Riddell	20	Equilibrium dissociated air	Sutherland	Constant	.76	.4
Kemp, Rose, and Detra	32	Equilibrium dissociated air	Sutherland	Constant	.793	.438
Cohen and Beckwith		Equilibrium dissociated air	Hansen, ref. 18	Variable, Hansen, ref. 18	.767	.45

TABLE II.- YAWED-INFINITE-CYLINDER STAGNATION-LINE LAMINAR HEAT TRANSFER

$$[N_{Le} = 1]$$

Solution	Reference	Gas	Transport properties		A	m
			μ	N_{Pr}		
Squire	33	Incompressible	Constant	Constant	0.570	0.5
Beckwith	31	Perfect compressible	Sutherland	Constant	.577	.44
Kemp, Rose, and Detra ^a	32	Equilibrium dissociated air	Sutherland	Constant	.576	.438
Cohen and Beckwith		Equilibrium dissociated air	Hansen, ref. 18	Variable, Hansen, ref. 18	.594	.5

^aSolutions for zero yaw only.

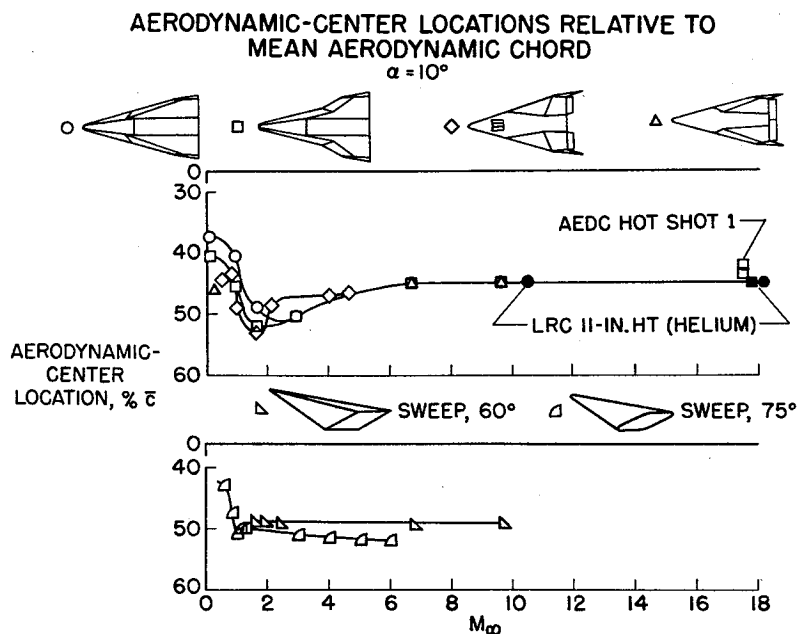


Figure 1

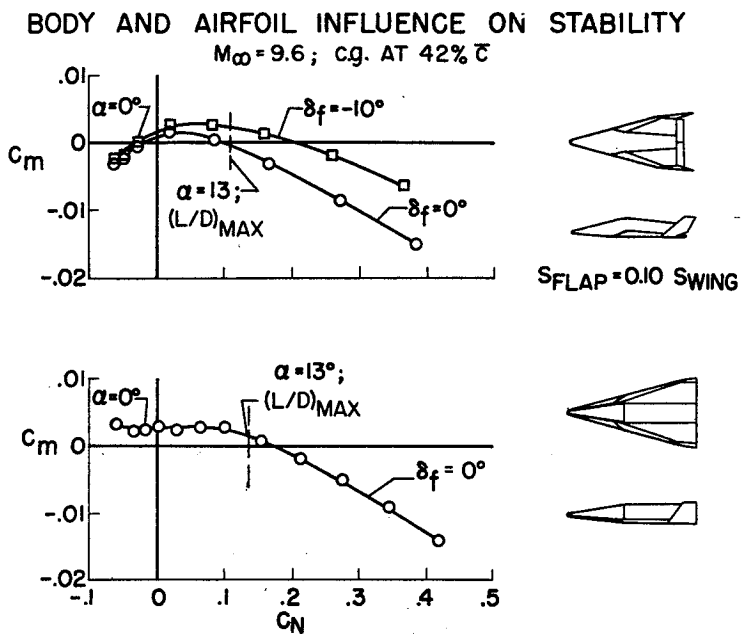


Figure 2

EFFECT OF FLAP DEFLECTION ON DELTA-WING CHARACTERISTICS

$M_\infty = 6.7$; c.g. AT 42% \bar{c} ; $S_{FLAP} = 0.19 S_{WING}$

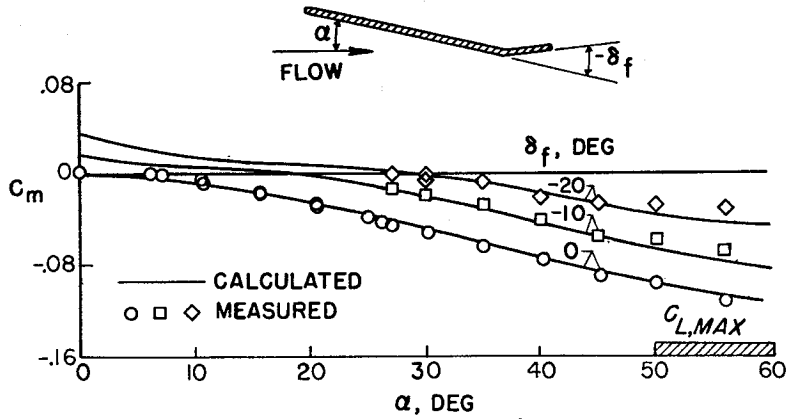


Figure 3

EFFECT OF NOSE DEFLECTION ON DELTA-WING CHARACTERISTICS

$M_\infty = 6.7$; c.g. AT 42% \bar{c} ; $S_{NOSE} = 0.16 S_{WING}$; $S_{FLAP} = 0.19 S_{WING}$

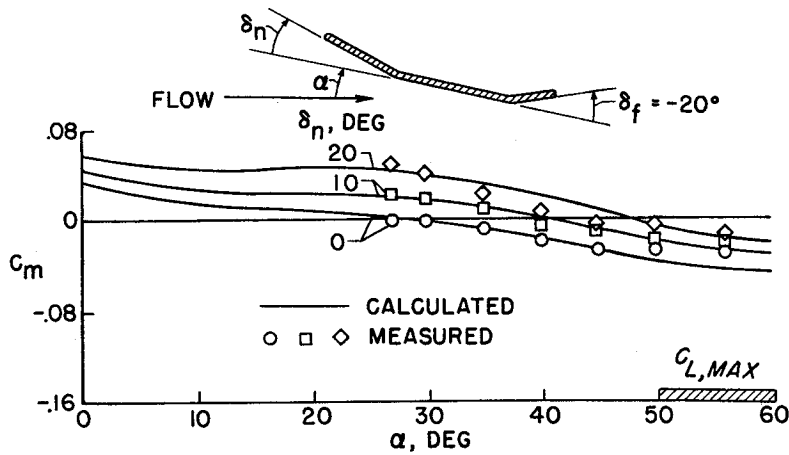


Figure 4

HIGH-ANGLE-OF-ATTACK LONGITUDINAL TRIM CHARACTERISTICS

$M_\infty = 6.7$; c.g. AT 42% \bar{c} ; $S_{NOSE} = 0.16 S_{WING}$; $S_{FLAP} = 0.19 S_{WING}$

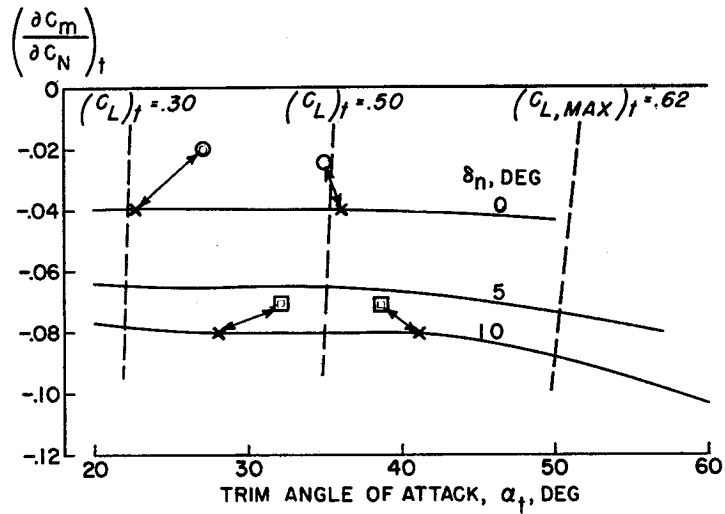


Figure 5

COMPUTED HIGH-ANGLE-OF-ATTACK LONGITUDINAL TRIM CHARACTERISTICS

$M_\infty = 18$; c.g. AT 42% \bar{c} ; $S_{NOSE} = 0.16 S_{WING}$; $S_{FLAP} = 0.19 S_{WING}$

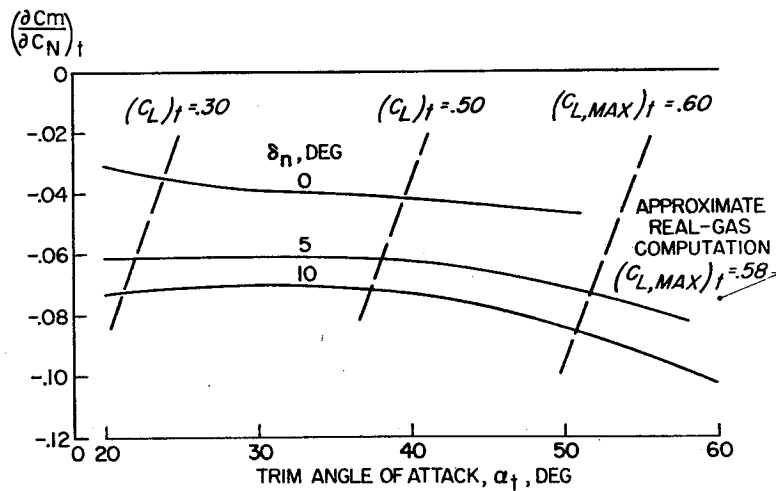


Figure 6

MACH NUMBER EFFECT ON DIRECTIONAL AND LATERAL STABILITY

$\alpha = 10^\circ$

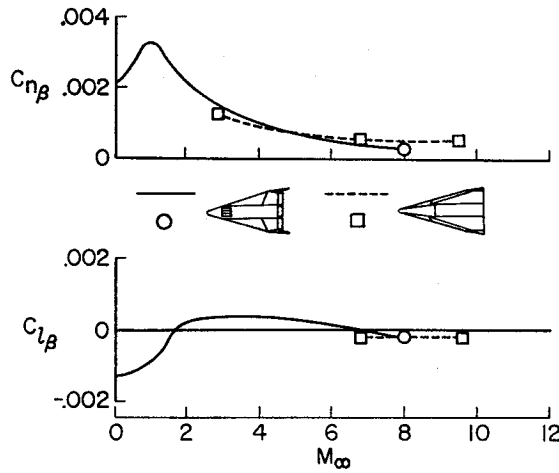


Figure 7

ANGLE-OF-ATTACK EFFECT ON DIRECTIONAL AND LATERAL STABILITY

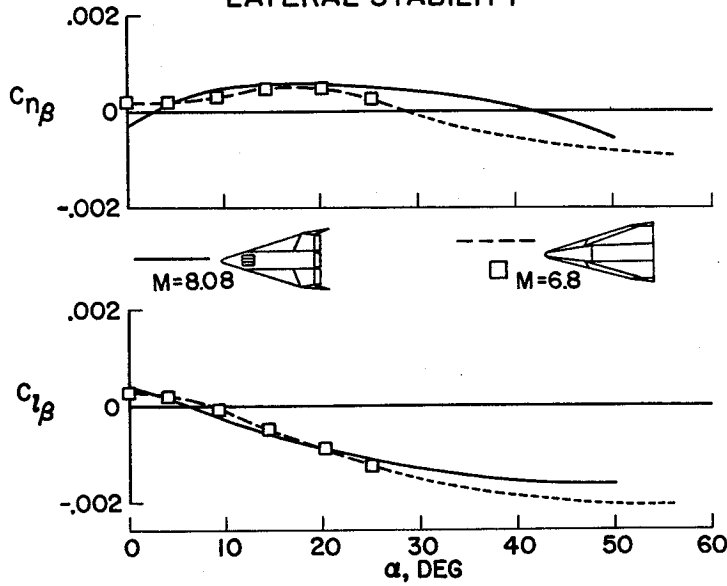


Figure 8

EFFECTS OF FIN ROLLOUT ON DIRECTIONAL STABILITY
 $S_{FIN} = 0.08S_{WING}$; $S_{FLAP} = 0.19S_{WING}$

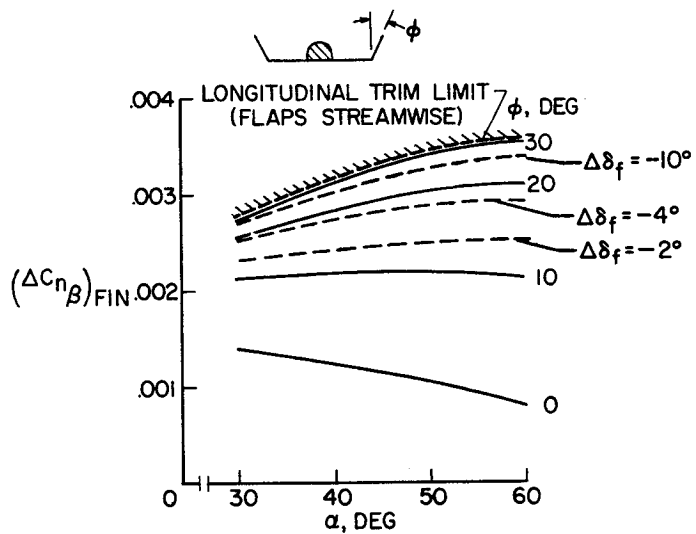


Figure 9

[REDACTED]

[REDACTED]